Geophysical Research Letters

RESEARCH LETTER
10.1029/2019GL083550

Consistent Nighttime Atomic Oxygen Concentrations From O_2 A-band, $O(^1S)$ Green-Line, and OH Airglow Measurements as Performed by SCIAMACHY

Yajun Zhu[1] **and Martin Kaufmann**[1,2]

[1]Institute of Energy and Climate Research, Forschungszentrum Jülich, Jülich, Germany, [2]Institute for Atmospheric and Environmental Research, University of Wuppertal, Germany

Key Points:
- A new atomic oxygen data set is derived from SCIAMACHY O_2 A-band nightglow measurements
- Good agreement is found between three atomic oxygen data sets from SCIAMACHY
- The agreement between the various data sets supports current understanding of retrieval models for the derivation of atomic oxygen

Supporting Information:
- Text S1

Correspondence to:
M. Kaufmann,
m.kaufmann@fz-juelich.de

Citation:
Zhu, Y., & Kaufmann, M. (2019). Consistent nighttime atomic oxygen concentrations from O_2 A-band, $O(^1S)$ green line, and OH airglow measurements as performed by SCIAMACHY. *Geophysical Research Letters*, *46*, 8536–8545. https://doi.org/10.1029/2019GL083550

Received 3 MAY 2019
Accepted 10 JUL 2019
Accepted article online 16 JUL 2019
Published online 30 JUL 2019

©2019. The Authors.
This is an open access article under the terms of the Creative Commons Attribution-NonCommercial-NoDerivs License, which permits use and distribution in any medium, provided the original work is properly cited, the use is non-commercial and no modifications or adaptations are made.

Abstract A new atomic oxygen data set was derived from nighttime SCanning Imaging Absorption spectroMeter for Atmospheric CHartographY (SCIAMACHY) O_2 A-band measurements. It is compared to atomic oxygen obtained from SCIAMACHY $O(^1S)$ green-line and OH(9-6)-band measurements. The three data sets are considered independent of radiometry and, to some extent, methodology. A detailed comparison of atomic oxygen retrieved from these three nightglow measurements is reported for the first time. The agreement of absolute values within 15% supports the current understanding of the photochemistry of the three atomic oxygen proxies involved. As an alternative approach, the O_2 A-band model recently proposed by Kalogerakis (2019) is used as well. It is striking that the SCIAMACHY data sets using different atomic oxygen proxies and mostly independent methodology agree much better with each other than with SABER data.

1. Introduction

Atomic oxygen plays a crucial role in the photochemistry and energy balance of the upper mesosphere and lower thermosphere (UMLT) region (Brasseur & Offermann, 1986; Riese et al., 1994). An accurate knowledge of atomic oxygen abundance is also important for the derivation of other atmospheric quantities, which are in nonlocal thermodynamic equilibrium.

Global measurements of atomic oxygen in the UMLT rely on species involved in the photochemistry of atomic oxygen, such as ozone or the various excited states of the hydroxyl radical, molecular, and atomic oxygen. One key reaction in this context is the three-body recombination reaction of atomic oxygen ($O+O+M \rightarrow O_2^*+M$) leading to highly excited molecular oxygen O_2^*. Atomic and molecular oxygen can be excited by collisions with this metastable state. Another key reaction in the UMLT is the exothermic reaction of H and O_3 ($H+O_3 \rightarrow O_2+OH^*$) resulting in vibrationally excited OH^*. These excited products radiate nightglow and dayglow. Over the last few decades, spectroscopic techniques have been common methods measuring these species globally with atomic oxygen concentrations being derived from these data by means of photochemical models (Kaufmann et al., 2014; Mlynczak et al., 2018; Panka et al., 2018; Russell et al., 2005; Sheese et al., 2011; Zhu & Kaufmann, 2018). The $O(^1S)$ green-line, O_2 A-band, and OH Meinel band emissions are frequently used as proxies for atomic oxygen. $O(^1S)$ green-line nightglow was measured using the Wind Imaging Interferometer instrument from 1991 to 1997 (Russell et al., 2005) and using the Imager of Sprites and Upper Atmospheric Lightning instrument (Gao et al., 2012). O_2 A-band dayglow and nightglow measurements have been performed by the Optical Spectrograph and Infrared Imager System instrument since 2002 (Sheese et al., 2011). OH Meinel band emissions have been measured by the Sounding of the Atmosphere using Broadband Emission Radiometry (SABER) instrument since 2002 (Smith et al., 2010).

Atomic oxygen concentrations in the UMLT have been derived from several satellite measurements (Kaufmann et al., 2014; Mlynczak et al., 2013; Russell et al., 2005; Sheese et al., 2011; Smith et al., 2010). These measurements are difficult to compare, because they were not simultaneously observed or were made at different locations and local times. A difference of up to 60% was found by comparing atomic oxygen abundance derived from SABER 2.0 μm OH and from SCIAMACHY (SCanning Imaging Absorption spectroMeter for Atmospheric CHartographY) $O(^1S)$ green-line measurements (Kaufmann et al., 2014). The large discrepancy in values has reignited discussions about the absolute values of atomic oxygen abundance and the photochemistry of emitting species (Mlynczak et al., 2018; Panka et al., 2018). New atomic oxygen

data were retrieved from SABER 2.0-μm absolute radiance measurements by enlarging/reducing collisional rate constants within the constraints of the annual global mean energy budget in the UMLT (Mlynczak et al., 2018). In comparison with other atomic oxygen data sets obtained by Kaufmann et al. (2014) and Zhu and Kaufmann (2018), the agreement of the newly derived SABER data is significantly better than the previous SABER data derived by Mlynczak et al. (2013). However, systematic differences of up to 50% still persist (Zhu & Kaufmann, 2018), especially when consistent forward model parameters are used (Zhu & Kaufmann, 2018). Using a completely different approach, Panka et al. (2018) also retrieved atomic oxygen from ratios of SABER OH 1.6- and 2.0-μm radiance measurements. A bias of less than 20% compared with other data was found, but a detailed comparison has yet to be made.

SCIAMACHY on board Envisat (Environmental Satellite) is an eight-channel grating spectrometer covering a wavelength range from the ultraviolet to the near-infrared spectral region. Nighttime O(^{1}S) green-line, O_2 A-band, and OH(9-6)-band emissions were simultaneously measured by SCIAMACHY Channels 3, 4, and 6, respectively. These data offer us a clear opportunity to investigate atomic oxygen abundance and our current understanding of the photochemistry of the emitting species. Two atomic oxygen data sets were derived from O(^{1}S) green-line and OH(9-6)-band emission measurements (Kaufmann et al., 2014; Zhu & Kaufmann, 2018). The vertical coverage of these data ranges from an altitude of 80–93 km for the derivation from OH data to an altitude of 90–105 km for the O(^{1}S) green-line data. The overlapping region is therefore about 3 km. The agreement of the two data sets is within 10–20% in the overlapping region. SCIAMACHY O_2 A-band measurements provide a further basis for investigating the above-mentioned issues, with additional information on atomic oxygen derivation and a comparison covering an altitude region from 83 to 102 km.

2. O_2 A-Band Nightglow Modeling

O_2 A-band nightglow originates from spontaneous emissions, qualified by the Einstein coefficient A_{762}, of $O_2(b^1\Sigma_g^+, v = 0)$ stemming from a two-step Barth mechanism (Barth & Hildebrandt, 1961) during nighttime in the absence of aurora. The following two reactions are involved:

$$O + O + M \rightarrow O_2^* + M, \tag{1}$$

$$O_2^* + O_2\ (+O) \rightarrow O_2(b^1\Sigma_g^+, v = 0, 1, 2) + O_2\ (+O(^1D)), \tag{2}$$

where M represents O_2 or N_2. O_2^* in reaction (1) represents any of the seven lowest bound electronic metastable states below O_2 photo-dissociation limit, that is, $^5\Pi_g$, $A^3\Sigma_u^+$, $A'^3\Delta_u$, $c^1\Sigma_u^-$, $b^1\Sigma_g^+$, $a^1\Delta_g$, and $X^3\Sigma_g^-$ from high to low levels of its electronic state (Slanger & Copeland, 2003). Airglow measurements and laboratory experiments indicate that reaction (1) produces only a small fraction of $O_2(b^1\Sigma_g^+)$ molecules directly. Instead, additional collisions with ground state O_2 or O (reaction (2)) produce most of the molecules in that state (Grygalashvyly et al., 2019; Kalogerakis, 2019; Pejaković et al., 2007). The production rate of $O_2(b^1\Sigma_g^+)$ can be expressed as (Kalogerakis, 2019)

$$P_{O_2^b} = \frac{f_{O_2^*} \cdot k_{OOM} \cdot [O]^2 \cdot [O_2] \cdot [M] \cdot (f_{O_2} \cdot k_{O_2^*O_2} \cdot [O_2] + f_O \cdot k_{O_2^*O} \cdot [O])}{A_{O_2^*} + k_{O_2^*O} \cdot [O] + k_{O_2^*O_2} \cdot [O_2] + k_{O_2^*N_2} \cdot [N_2]}. \tag{3}$$

Chemical species denoted in the equation by square brackets represent their corresponding volume number densities. $f_{O_2^*}$ is the yield rate to produce O_2^* in reaction (1). f_{O_2} and f_O are the corresponding yield rates producing $O_2(b^1\Sigma_g^+)$ in reaction (2), respectively. k_{OOM} is the rate constant of reaction (1) producing O_2^*. $A_{O_2^*}$ is the Einstein coefficient qualifying the lifetime of O_2^*. $k_{O_2^*N_2}$, $k_{O_2^*O_2}$, and $k_{O_2^*O}$ are collisional removal rates of O_2^* by N_2, O_2, and O, respectively. To reduce the number of rate constants used in equation (3), McDade et al. (1986) derived the following expression:

$$P_{O_2^b} = \frac{k_{OOM} \cdot [O]^2 \cdot [O_2] \cdot [M]}{C_O \cdot [O] + C_{O_2} \cdot [O_2]}. \tag{4}$$

The empirical parameters C_O and C_{O_2} were obtained by simultaneous observations of atomic oxygen resonance fluorescence and O_2 A-band data during the ETON campaign (McDade et al., 1986). Since this method relies on some a priori information of the background atmosphere, McDade et al. (1986) gave two sets of

Table 1
Quenching Rate Constants of the O_2 A-Band Model

Rate	Value	Reference
k_{OOM}	$4.7 \times 10^{-33}(300/T)^2$ cm^6/s	Campbell and Gray (1973)
C_{O_2}	(5.7 ± 0.4)	McDade et al. (1986)
C_O	(17 ± 2)	McDade et al. (1986)
$k_{O_2^bO}$	$(8.0 \pm 2.0) \times 10^{-14}$ cm^3/s	Burkholder et al. (2015)
$k_{O_2^bO_2}$	$(7.4 \pm 0.8) \times 10^{-17} \times T^{0.5} \times e^{\frac{(-1104.7 \pm 53.3)}{T}}$ cm^3/s	Zagidullin et al. (2017)
$k_{O_2^bN_2}$	$(8.0 \pm 0.3) \times 10^{-20} \times T^{1.5} \times e^{\frac{(503 \pm 21)}{T}}$ cm^3/s	Zagidullin et al. (2017)
A_{762}	0.0878 s^{-1} at 200 K	This work
$A_{b\Sigma}$	0.0925 s^{-1} at 200 K	This work

these parameters based on the CIRA 1972 (COSPAR, 1972) and MSIS-83 (Hedin, 1983) reference atmospheres, respectively. In this study, we use an average value of the two pairs (17 and 5.7, respectively; see Table 1).

The Einstein coefficient $A_{b\Sigma}$ of $O_2(b^1\Sigma_g^+, v = 0 \rightarrow X^3\Sigma_g^-)$ is 0.0925 s^{-1} and the corresponding radiative lifetime of $O_2(b^1\Sigma_g^+, v = 0)$ is about 11 s, which is much longer than the typical time scales to relax the superposed vibrational excitation of this state (Bucholtz et al., 1986; Sheese, 2009). Therefore, almost all molecules $O_2(b^1\Sigma_g^+)$ produced in reaction (2) end up in $O_2(b^1\Sigma_g^+, v = 0)$. The long lifetime of this state also implies that the rotational excitation of this state is fully thermalized with the ambient atmosphere. $O_2(b^1\Sigma_g^+, v = 0)$ can be considered in rotational equilibrium in the UMLT. Assuming $O_2(b^1\Sigma_g^+, v = 0)$ to be in a steady state, the O_2 A-band volume emission rate V_A can be quantified by multiplying the Einstein coefficient A_{762} and the ratio of the $O_2(b^1\Sigma_g^+, v = 0)$ production and loss rates.

$$V_A = \frac{A_{762} \cdot P_{O_2^b}}{(A_{b\Sigma} + k_{O_2^bO} \cdot [O] + k_{O_2^bO_2} \cdot [O_2] + k_{O_2^bN_2} \cdot [N_2])} \tag{5}$$

$k_{O_2^bO}$, $k_{O_2^bO_2}$, and $k_{O_2^bN_2}$ are the quenching rates for the collisional deactivation of $O_2(b^1\Sigma_g^+, v = 0)$ by O, O_2, and N_2, respectively. The collisional rate constants used in the model are given in Table 1. Different Einstein coefficients of O_2 A-band and $O_2(b^1\Sigma_g^+, v = 0 \rightarrow X^3\Sigma_g^-)$ have been used in the community (Grygalashvyly et al., 2019; Kalogerakis, 2019; Sheese, 2009) and the two Einstein coefficients are calculated based on the HITRAN spectroscopic database (Gordon et al., 2017) in this study.

Based on the equations discussed above, a forward model to simulate O_2 A-band limb emission rates is developed to retrieve atomic oxygen abundance iteratively from O_2 A-band measurements obtained by the SCIAMACHY instrument. For the simulation of limb radiances, self-absorption within the O_2 A-band is considered. O_2 A-band absorption cross-sections along the line of sight are calculated line by line with a wave number sampling of 0.001 cm^{-1} in the A band. The weighted average band transmissions can then be determined. At the bottom of the emission layer (80 km), more than 25% of the emitted photons cannot reach the instrument due to self-absorption.

3. SCIAMACHY O_2 A-Band Nightglow Measurements and Retrieval Results

O_2 nightglow limb measurements were performed by SCIAMACHY from 2002 to 2012. SCIAMACHY performed measurements from a sun-synchronous polar orbit with an ascending node at a local solar time of 10 p.m. For the following study, we use O_2 A-band nightglow data observed by SCIAMACHY Channel 4 in a spectral range from 758 to 768 nm (Figure 1) at a spectral resolution of 0.48 nm. This spectral region covers all O_2 A-band emissions. The O_2 A-band individual rotational lines cannot be resolved due to the low spectral resolution and integrated O_2 A-band limb radiances are used in this work. In order to enhance the signal-to-noise ratio, monthly zonal median data in 5° latitude bins are used in this study. Since the SCIAMACHY instrument cannot measure nighttime temperature or total density in the UMLT, colocated SABER measurements (v2.0) are used here. The coincidence criteria are ±2.5° in latitude and 1 hr in local time.

A constrained global fit retrieval technique is applied to obtain vertical profiles of atomic oxygen abundance between 83 and 102 km (Kaufmann et al., 2014). Regularization was adjusted in such a way that the vertical

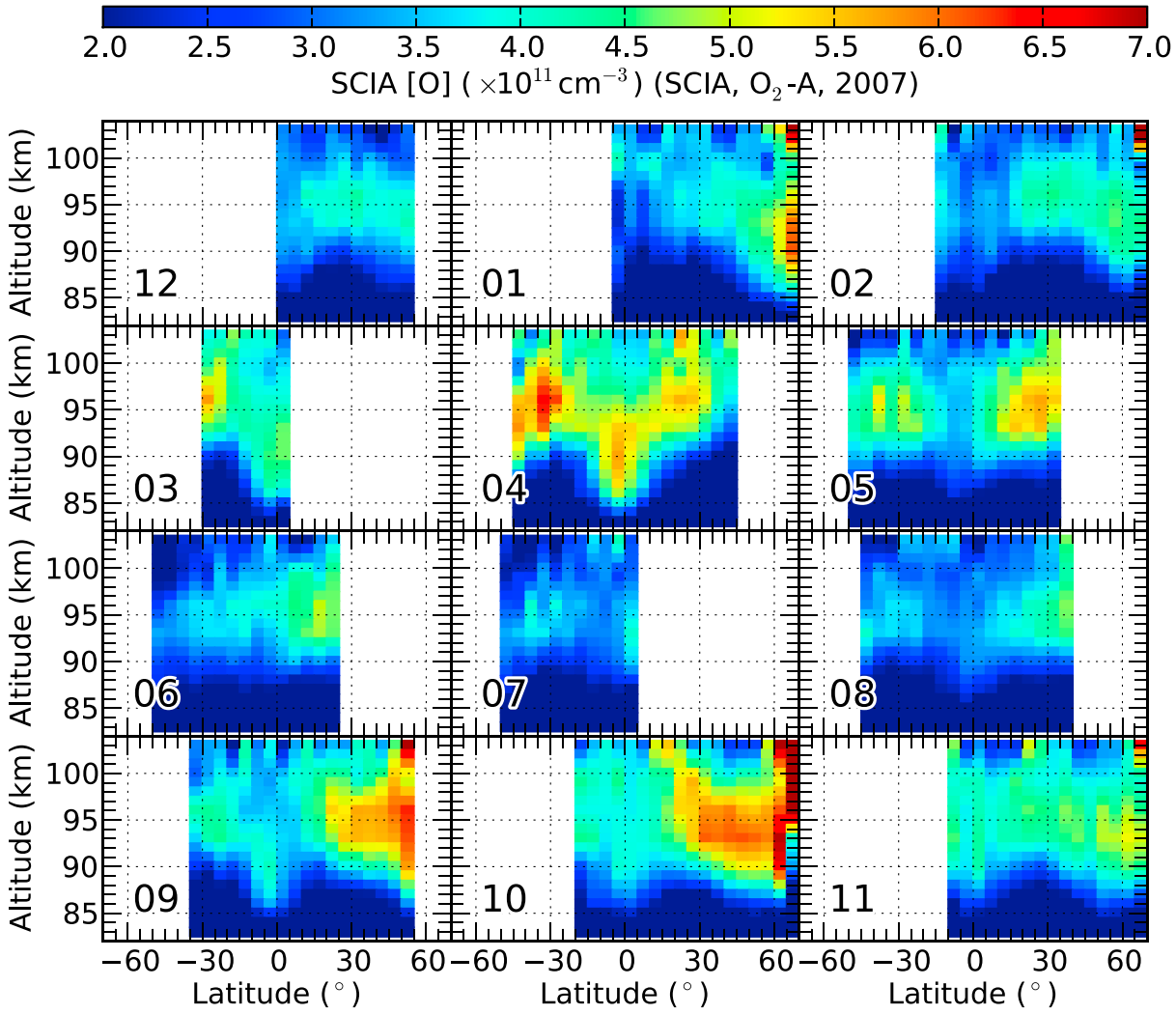

Figure 3. Monthly zonal mean global atomic oxygen abundance for 2007, as derived from SCanning Imaging Absorption spectroMeter for Atmospheric CHartographY O_2 A-band nightglow measurements. The numbers represent the month of the year 2007.

uncertainty increasing from around 4% at 83 km to about 17% at 103 km. Overall atomic oxygen uncertainty thus increases from about 10% at 83 km to 20% at 100 km, increasing rapidly to 26% at 103 km.

Figure 2 shows comparisons between the retrieved atomic oxygen profiles and the atomic oxygen data obtained from SCIAMACHY green-line and OH nightglow measurements at 20–40° N for September 2005 and September 2009 (Kaufmann et al., 2014; Zhu & Kaufmann, 2018; Zhu et al., 2015). Uncertainties of atomic oxygen retrieved from SCIAMACHY green-line and OH nightglow measurements are about 13–15% and 17–21%, respectively. This is due to uncertainties of related rate constants and auxiliary atmospheric quantities. For details, please refer to the work of Zhu et al. (2015) and Zhu and Kaufmann (2018). The newly derived atomic oxygen data set almost overlaps with the other two data sets in the altitude regime of 83–103 km and agrees with these data sets to within 10%, as shown in Figure 2. A retrieval was performed using a new pair of empirical parameters C_O and C_{O_2} provided by Grygalashvyly et al. (2019) based on a self-consistent rocket-borne experiment conducted in 2015 and the new parameters increase retrieved atomic oxygen abundance by about 33% at around 87 km. After reanalyzing the ETON rocket measurements (Murtagh et al., 1990), Kalogerakis (2019) gave an evidence for an additional nighttime O_2^* source stemming from the collision of O_2 and $O(^1D)$. He proposed that $O(^1D)$ is generated through the quenching of $OH(\nu \geq 5)$ by atomic oxygen. Since SCIAMACHY measured highly excited OH as well, this process can be included straight forward in the model. We follow Kalogerakis (2019) by including collisions between $OH(\nu = 9)$ and atomic oxygen only, which can be considered as a lower boundary for the generation of $O(^1D)$. We

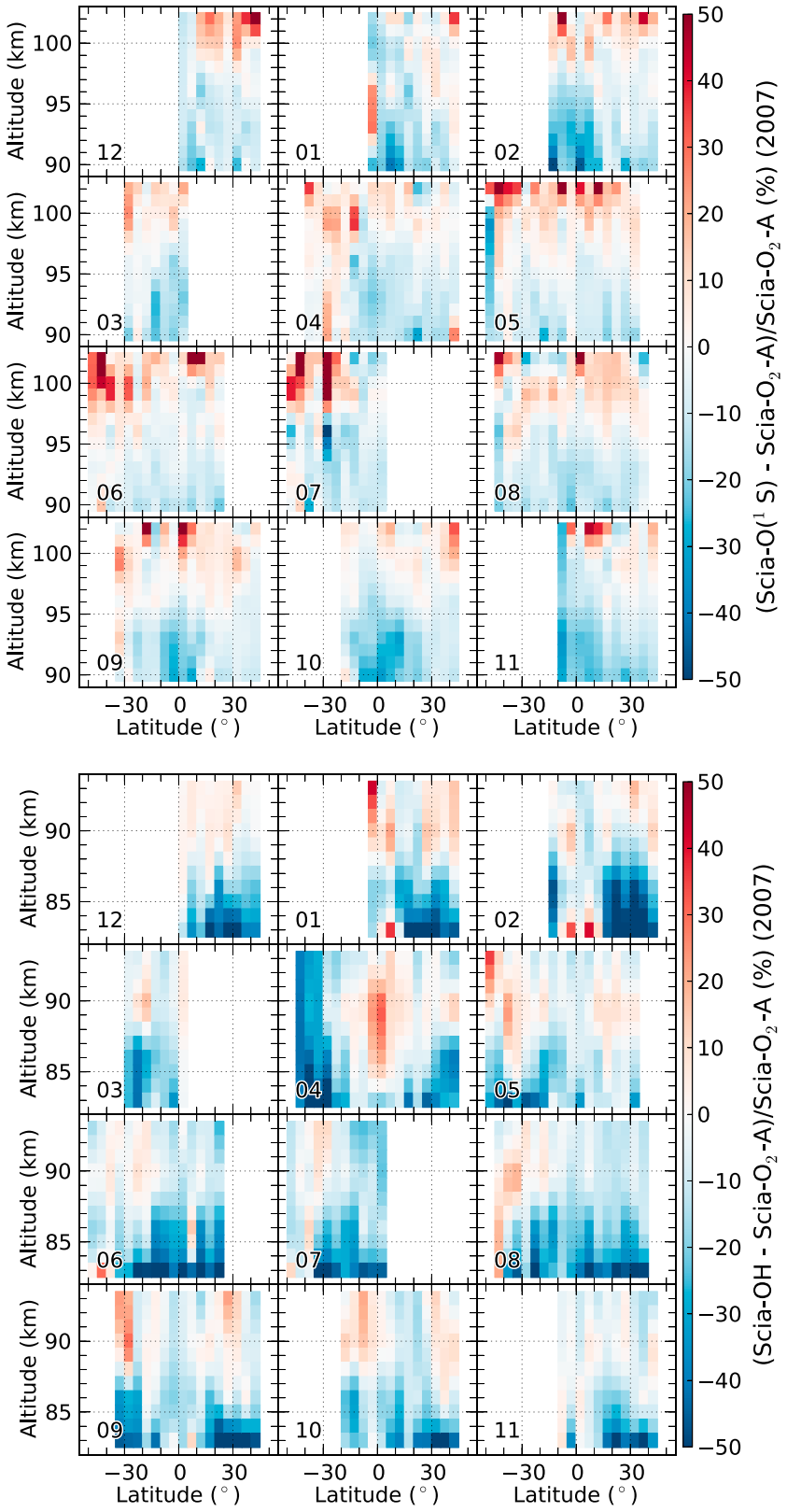

Figure 4. Percentage difference of SCanning Imaging Absorption spectroMeter for Atmospheric CHartographY (SCIAMACHY) atomic oxygen data for 2007, as derived from SCIAMACHY O(^{1}S) green-line and O_2 A-band measurements (top) and as derived from SCIAMACHY O_2 A-band and OH(9-6) band data (bottom). The numbers represent the month of the year 2007.

also include the modifications of rate constants made in the same study to build a similar forward model as Kalogerakis (2019). f_{O_2} and f_O in equation (4), which describe the production rate of $O_2(b^1\Sigma_g^+)$ due to collisions of O_2^* by O_2 and O, are 0.24 and 0.11, respectively. As shown in Figure 2, these modifications of the O_2 A-band model affect retrieved atomic oxygen abundance by less than 10% below 90 km, and somewhat more above to about 27% at 93 km, which is the highest altitude of reasonable signal-to-noise ratio of monthly mean SCIAMACHY OH(9-6) radiance data used for deriving OH($\nu = 9$) number densities. As pointed out by Kalogerakis (2019), more work is still needed to clarify details of the three-body reaction mechanism and contributions from collisions of OH($5 \leq \nu \leq 8$) and O, a discussion of which is beyond the scope of this study. SABER atomic oxygen as data derived by Mlynczak et al. (2018) is also given. Above 90 km, the SABER data agree within 10% with SCIAMACHY data, but lower values are found for the SABER data by a factor of 2 with respect to SCIAMACHY data below this altitude.

A global distribution of the new atomic oxygen data is illustrated in Figure 3 for the year 2007. The data cover the same period as the atomic oxygen data retrieved from SCIAMACHY O(^{1}S) data (Figure 3) of Kaufmann et al. (2014) and from SCIAMACHY OH(9-6) band data (Figure 4) of Zhu and Kaufmann (2018). Differences between the new dataset and the atomic oxygen data obtained from O(^{1}S) (Figure 4 (top)) are less than 10% on average (a mean value). The new atomic oxygen data show larger values of up to 30% over equator regions below atomic oxygen peak altitudes and tend to be 10-30% smaller on average above peak altitudes in comparison to atomic oxygen derived from SCIAMACHY O(^{1}S) green-line measurements. Differences of up to 50% are also found at some latitudes above 100 km. Figure 4 (bottom) indicates that the deviation is less than 15% on average. Positive biases of up to 30% are found at around 90 km over equator region in April and at about 30° S in September. A large negative bias of up to 40% is observed in February below 87 km at about 30° N, and in April at midlatitudes in the southern hemisphere. Kulikov et al. (2019) highlights that atomic oxygen, as derived from vibrationally excited OH, obtains a large uncertainty at low altitudes due to a breakdown in the chemical equilibrium of ozone production and loss during nighttime. We applied their criteria to the data presented in this work to evaluate whether this could explain the differences between the atomic oxygen datasets based on O_2 A-band and OH emissions. We found that the differences in this work are far above the boundary layer given in their work and that the differences found in this work are likely caused by other reasons.

Figure 5 (top) presents a global comparison of atomic oxygen derived from SCIAMACHY O_2 A-band measurements based on the photochemical model used in this work and the one proposed by Kalogerakis (2019). The differences between the two are less than 15% in general, but a positive bias of up to 30% is found at midlatitudes above 90 km in spring and autumn equinox seasons. A comparison of the new data set to the SABER atomic oxygen data obtained by Mlynczak et al. (2018) is also made within the context of a global perspective for the year 2007, as shown in Figure 5 (bottom). Deviations between the two data sets are about 30% on average above 92 km, but a large negative bias of over 50% is found below 88 km. Similar spatial structures of bias are found in a global view, and regions with a negative bias over 50% spread at altitudes below 90 km, in comparison to the data (Figure 5) of Zhu and Kaufmann (2018). The lower SABER data are most likely due to the low quenching rate constants of OH($\nu = 8$) used for the SABER atomic oxygen derivation at lower altitudes. It is still difficult to find an explanation for the difference at higher altitudes. A detailed analysis of SABER and SCIAMACHY radiance measurements is inevitably required since the significant differences between their products are found in both this work and the work published by Zhu and Kaufmann (2018). A profound discussion on this matter is beyond the scope of this study.

4. Conclusions

Three atomic oxygen data sets were derived from nightglow at various wavelengths emitted from different excited atoms or molecules. Since these data were observed in different channels of SCIAMACHY, it can be considered as mostly independent information in terms of radiometry. The excitation of the species involved relies on mostly independent photochemistry, except for O(^{1}S) and $O_2(b^1\Sigma_g^+, \nu = 0)$, which are excited by the three-body recombination reaction (1). The 30% uncertainty of the three-body recombination reaction maps linearly into the volume emission rates of the O(^{1}S) green line and O_2 A band and, ultimately, accounts for percentages in the order of 43–50% and 38–58%, respectively, of the overall uncertainties of atomic oxygen abundance. About half of the retrieval uncertainty stems from the same three-body recombination reaction. The derivation of atomic oxygen from green-line and O_2 A-band measurements is based on the assumption of O(^{1}S) and $O_2(b^1\Sigma_g^+, \nu = 0)$ being in a steady state. The approaches for atomic oxygen derivation from

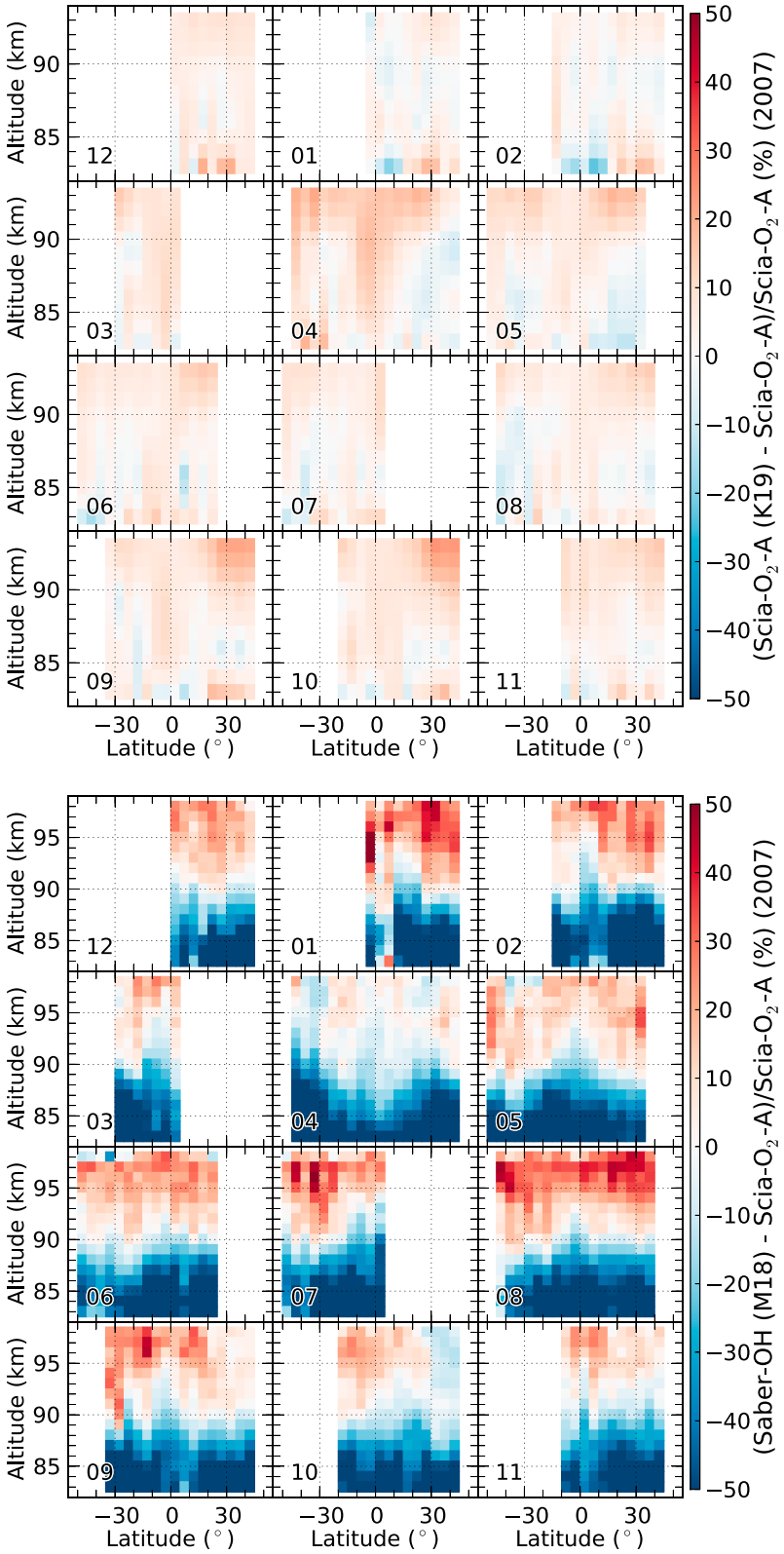

Figure 5. Percentage difference of SCanning Imaging Absorption spectroMeter for Atmospheric CHartographY (SCIAMACHY) atomic oxygen data for 2007, (top) as derived from SCIAMACHY O_2 A-band measurements using the model in this work and the one proposed by Kalogerakis (2019) and (bottom) as derived from SCIAMACHY O_2 A-band measurements and SABER OH 2.0-μm radiances by Mlynczak et al. (2018). The numbers represent the month of the year 2007.

green-line and A-band measurements are considered independently to some extent, although a systematic error might be inevitable for the data derived from green-line and A-band radiances. The comparison of these data sets indicates that the absolute value of atomic oxygen derived from SCIAMACHY measurements agrees to within 15%. This result supports our current understanding of the photochemistry of the corresponding emitting states, for example, the $O(^1S)$ green-line ETON model (McDade & Llewellyn, 1986), the O_2 A-band model used in this work, and the OH(9-6)-band emission model used by Zhu and Kaufmann (2018). Some empirical parameters used in the ETON model and the O_2 A-band model are taken from McDade et al. (1986). No significant systematic error is found using the ETON model and the O_2 A-band model applied in this work to derive atomic oxygen from SCIAMACHY $O(^1S)$ green-line and O_2 A-band measurements in comparison to the data obtained from SCIAMACHY OH radiance measurements.

A preliminary comparison is made for atomic oxygen data sets derived from SCIAMACHY O_2 A-band nightglow measurements using the photochemical model introduced in this work and the new model proposed by Kalogerakis (2019). Differences are less than 15% in general below 93 km, but a positive bias of up to 30% is found at 90–93 km over midlatitudes in equinox seasons. Deviations between SCIAMACHY atomic oxygen data and SABER data obtained by Mlynczak et al. (2018) are about 30% at altitudes above 92 km, but biases over 50% are found to be prominent below 90 km. The significant differences between the SCIAMACHY and SABER products emphasize the need for a further study on SCIAMACHY and SABER radiance data, which will be carried out in a separate investigation.

Acknowledgments
The work of Y. Zhu was supported by the 2017 Helmholtz-OCPC-Programme and the International Postdoctoral Exchange Fellowship Program 2017. M. Kaufmann was supported by Forschungszentrum Jülich. SCIAMACHY Level 1b Version 8 data used here are available at ftp://scia-ftp-ds.eo.esa.int. SABER Version 2.0 data are available at http://saber.gats-inc.com.

References

Barth, C. A., & Hildebrandt, A. F. (1961). The 5577 A airglow emission mechanism. *Journal of Geophysical Research*, *66*(3), 985–986. https://doi.org/10.1029/JZ066i003p00985

Brasseur, G., & Offermann, D. (1986). Recombination of atomic oxygen near the mesopause: Interpretation of rocket data. *Journal of Geophysical Research*, *91*(D10), 10,818–10,824. https://doi.org/10.1029/JD091iD10p10818

Bucholtz, A., Skinner, W., Abreu, V., & Hays, P. (1986). The dayglow of the O_2 atmospheric band system. *Planetary and Space Science*, *34*(11), 1031–1035. https://doi.org/10.1016/0032-0633(86)90013-9

Burkholder, J. B., Sander, S. P., Abbatt, J., Barker, J. R., Huie, R. E., Kolb, C. E., et al. (2015). Chemical kinetics and photochemical data for use in atmospheric studies, Evaluation No. 18. JPL Publication 15-10, JPL Publication 15-10.

COSPAR (1972). *CIRA 1972: COSPAR International Reference Atmosphere 1972*. Berlin: Akademie-Verlag.

Campbell, I., & Gray, C. (1973). Rate constants for $O(^3P)$ recombination and association with $N(^4S)$. *Chemical Physics Letters*, *18*(4), 607–609. https://doi.org/10.1016/0009-2614(73)80479-8

Dawkins, E. C. M., Feofilov, A., Rezac, L., Kutepov, A. A., Janches, D., Höffner, J., et al. (2018). Validation of SABER v2.0 operational temperature data with ground-based lidars in the mesosphere-lower thermosphere region (75 - 105 km). *Journal of Geophysical Research: Atmospheres*, *123*, 9916–9934. https://doi.org/10.1029/2018JD028742

Gao, H., Nee, J.-B., & Xu, J. (2012). The emission of oxygen green line and density of O atom determined by using ISUAL and SABER measurements. *Annales Geophysicae*, *30*(4), 695–701. https://doi.org/10.5194/angeo-30-695-2012

Gordon, I., Rothman, L., Hill, C., Kochanov, R., Tan, Y., Bernath, P., et al. (2017). The HITRAN2016 molecular spectroscopic database. *Journal of Quantitative Spectroscopy and Radiative Transfer*, *203*, 3–69. https://doi.org/10.1016/j.jqsrt.2017.06.038, HITRAN2016 Special Issue.

Grygalashvyly, M., Eberhart, M., Hedin, J., Strelnikov, B., Lübken, F.-J., Rapp, M., et al. (2019). Atmospheric band fitting coefficients derived from a self-consistent rocket-borne experiment. *Atmospheric Chemistry and Physics*, *19*(2), 1207–1220. https://doi.org/10.5194/acp-19-1207-2019

Hedin, A. E. (1983). A revised thermospheric model based on mass spectrometer and incoherent scatter data: Msis-83. *Journal of Geophysical Research*, *88*(A12), 10,170–10,188. https://doi.org/10.1029/JA088iA12p10170

Kalogerakis, K. S. (2019). A previously unrecognized source of the O_2 atmospheric band emission in earth's nightglow. *Science Advances*, *5*(3), eaau9255. https://doi.org/10.1126/sciadv.aau9255

Kaufmann, M., Zhu, Y., Ern, M., & Riese, M. (2014). Global distribution of atomic oxygen in the mesopause region as derived from SCIAMACHY $O(^1S)$ green line measurements. *Geophysical Research Letters*, *41*, 6274–6280. https://doi.org/10.1002/2014GL060574

Kulikov, M. Y., Nechaev, A. A., Belikovich, M. V., Vorobeva, E. V., Grygalashvyly, M., Sonnemann, G. R., & Feigin, A. M. (2019). Boundary of nighttime ozone chemical equilibrium in the mesopause region from SABER data: Implications for derivation of atomic oxygen and atomic hydrogen. *Geophysical Research Letters*, *46*, 997–1004. https://doi.org/10.1029/2018GL080364

McDade, I. C., & Llewellyn, E. J. (1986). The excitation of $O(^1S)$ and O_2 bands in the nightglow: A brief review and preview. *Canadian Journal of Physics*, *64*(12), 1626–1630. https://doi.org/10.1139/p86-287

McDade, I., Murtagh, D., Greer, R., Dickinson, P., Witt, G., Stegman, J., et al. (1986). ETON 2: Quenching parameters for the proposed precursors of $O_2(b^1\Sigma_g^+)$ and $O(^1S)$ in the terrestrial nightglow. *Planetary and Space Science*, *34*(9), 789–800. https://doi.org/10.1016/0032-0633(86)90075-9

Mlynczak, M. G., Hunt, L. A., Mast, J. C., Thomas Marshall, B., Russell, J. M., Smith, A. K., et al. (2013). Atomic oxygen in the mesosphere and lower thermosphere derived from SABER: Algorithm theoretical basis and measurement uncertainty. *Journal of Geophysical Research: Atmospheres*, *118*, 5724–5735. https://doi.org/10.1002/jgrd.50401

Mlynczak, M. G., Hunt, L. A., Russell, J. M., & Marshall, B. T. (2018). Updated SABER night atomic oxygen and implications for SABER ozone and atomic hydrogen. *Geophysical Research Letters*, *45*, 5735–5741. https://doi.org/10.1029/2018GL077377

Murtagh, D., Witt, G., Stegman, J., McDade, I., Llewellyn, E., Harris, F., & Greer, R. (1990). An assessment of proposed $O(^1S)$ and $O_2(b^1\Sigma_g^+)$ nightglow excitation parameters. *Planetary and Space Science*, *38*(1), 43–53. https://doi.org/10.1016/0032-0633(90)90004-A

Panka, P. A., Kutepov, A. A., Rezac, L., Kalogerakis, K. S., Feofilov, A. G., Marsh, D., et al. (2018). Atomic oxygen retrieved from the SABER 2.0- and 1.6-μm radiances using new first-principles nighttime OH(v) model. *Geophysical Research Letters*, *45*, 5798–5803. https://doi.org/10.1029/2018GL077677

Pejaković, D. A., Copeland, R. A., Cosby, P. C., & Slanger, T. G. (2007). Studies on the production of $O_2(a^1\Delta_g,\ v=0)$ and $O_2(b^1\Sigma_g^+),\ v=0)$ from collisional removal of $O_2(A^3\Sigma_u^+,\ v=6\text{ - }10)$. *Journal of Geophysical Research*, *112*, A10307. https://doi.org/10.1029/2007JA012520

Riese, M., Offermann, D., & Brasseur, G. (1994). Energy released by recombination of atomic oxygen and related species at mesopause heights. *Journal of Geophysical Research*, *99*(D7), 14,585–14,593. https://doi.org/10.1029/94JD00356

Russell, J. P., Ward, W. E., Lowe, R. P., Roble, R. G., Shepherd, G. G., & Solheim, B. (2005). Atomic oxygen profiles (80 to 115 km) derived from Wind Imaging Interferometer/Upper Atmospheric Research Satellite measurements of the hydroxyl and greenline airglow: Local time-latitude dependence. *Journal of Geophysical Research*, *110*, D15305. https://doi.org/10.1029/2004JD005570

Sheese, P. E. (2009). Mesospheric ozone densities retrieved from OSIRIS observations of the O_2 A-band dayglow (Ph.D. thesis).

Sheese, P. E., McDade, I. C., Gattinger, R. L., & Llewellyn, E. J. (2011). Atomic oxygen densities retrieved from Optical Spectrograph and Infrared Imaging System observations of O_2 A-band airglow emission in the mesosphere and lower thermosphere. *Journal of Geophysical Research*, *116*, D01303. https://doi.org/10.1029/2010JD014640

Slanger, T. G., & Copeland, R. A. (2003). Energetic oxygen in the upper atmosphere and the laboratory. *Chemical Reviews*, *103*(12), 4731–4766. https://doi.org/10.1021/cr0205311

Smith, A. K., Marsh, D. R., Mlynczak, M. G., & Mast, J. C. (2010). Temporal variations of atomic oxygen in the upper mesosphere from SABER. *Journal of Geophysical Research*, *115*, D18309. https://doi.org/10.1029/2009JD013434

Smith, G. P., & Robertson, R. (2008). Temperature dependence of oxygen atom recombination in nitrogen after ozone photolysis. *Chemical Physics Letters*, *458*(1-3), 6–10. https://doi.org/10.1016/j.cplett.2008.04.074

Zagidullin, M. V., Khvatov, N. A., Medvedkov, I. A., Tolstov, G. I., Mebel, A. M., Heaven, M. C., & Azyazov, V. N. (2017). $O_2(b^1\Sigma_g^+)$ quenching by O_2, CO_2, H_2O, and N_2 at temperatures of 300-800 K. *The Journal of Physical Chemistry A*, *121*(39), 7343–7348. https://doi.org/10.1021/acs.jpca.7b07885

Zhu, Y., & Kaufmann, M. (2018). Atomic oxygen abundance retrieved from SCIAMACHY hydroxyl nightglow measurements. *Geophysical Research Letters*, *45*, 9314–9322. https://doi.org/10.1029/2018GL079259

Zhu, Y., Kaufmann, M., Ern, M., & Riese, M. (2015). Nighttime atomic oxygen in the mesopause region retrieved from SCIAMACHY $O(^1S)$ green line measurements and its response to solar cycle variation. *Journal of Geophysical Research: Space Physics*, *120*, 9057–9073. https://doi.org/10.1002/2015JA021405